

A fast method for particle picking in cryo-electron micrographs based on fast R-CNN

Yifan Xiao, and Guangwen Yang

Citation: AIP Conference Proceedings **1836**, 020080 (2017); doi: 10.1063/1.4982020

View online: <https://doi.org/10.1063/1.4982020>

View Table of Contents: <http://aip.scitation.org/toc/apc/1836/1>

Published by the American Institute of Physics

Articles you may be interested in

Preface: 2017 International Conference on Applied Mathematics and Computer Science (ICAMCS 2017)
AIP Conference Proceedings **1836**, 010001 (2017); 10.1063/1.4981940

[Human vehicle interaction](#)

AIP Conference Proceedings **1836**, 020050 (2017); 10.1063/1.4981990

[Deterministic decomposition and seasonal ARIMA time series models applied to airport noise forecasting](#)
AIP Conference Proceedings **1836**, 020079 (2017); 10.1063/1.4982019

[Conservation laws of one-dimensional strain-limiting viscoelasticity model](#)

AIP Conference Proceedings **1836**, 020081 (2017); 10.1063/1.4982021

[Content-level deduplication on mobile internet datasets](#)

AIP Conference Proceedings **1836**, 020086 (2017); 10.1063/1.4982026

[An effective convolutional neural network model for Chinese sentiment analysis](#)

AIP Conference Proceedings **1836**, 020085 (2017); 10.1063/1.4982025

A Fast Method for Particle Picking in Cryo-Electron Micrographs based on Fast R-CNN

Yifan Xiao^{1,a)} and Guangwen Yang^{1,b)}

¹School of Computer Science and Technology, Tsinghua University, Beijing, 100084, China

^{a)}xjf14@mails.tsinghua.edu.cn
^{b)}ygw@tsinghua.edu.cn

Abstract. We propose a fast method to automatically pick protein particles in cryo-EM micrographs, which is now completed manually in practice. Our method is based on Fast R-CNN, with sliding window as the regions proposal solution. To reduce the false positive detections, we set a single class for the major contaminant ice, and pick out all the ice particles in the whole datasets. Tests on the recently-published cryo-EM data of three proteins have demonstrated that our approach can automatically accomplish the human-level particle picking task, and we successfully reduce the test time from 1.5 minutes of previous deep learning method to 2 seconds without any recall or precision losses. Our program is available under the MIT License at <https://github.com/xiaofan/FastParticlePicker>.

INTRODUCTION

In recent years, with the improvements of cryo-Electron-Microscope (cryo-EM)[1, 2], the structural analysis of protein complex has experienced tremendous breakthroughs[3, 4, 2, 5]. However, achieving such near-atomic resolution results usually requires hundreds of thousands of protein particle images, which are typically picked out from thousands of micrographs manually[6, 7]. This paper proposes a fast method to pick out particles automatically in about 2 seconds per micrograph.

For the protection of protein particles, biologists have to use low electron exposures and low defocus settings when taking a picture, making the micrographs in very low contrast[8]. The traditional image processing technologies cannot be easily applied to these blurred images, thus the particles are in practice picked manually, and this labor-intensive step can cost researchers several days to obtain a sufficient amount of good-quality particles. But better resolutions need more protein particles, and manual selection of particles is becoming a bottleneck for the application of cryo-EM in structural biology field[1, 9].

In order to minimize the labor cost during the micrograph data analysis, considerable efforts have been made to develop algorithms that automatically, or semi-automatically localize particles in these dim blurred micrographs. 1) In the early 2000s, the dominant particle picking methods rely on the template matching which attempts to identify particles in micrographs based on their similarities to reference templates[10, 11, 12, 13, 14]. In [13] they find a fast way to compute the similarities, in [11] they construct a profile of templates to reflect the characteristics of different angles, and in [10] they represent the templates with feature vectors instead of pixels. The innate flaw of these methods is the assumption that the three-dimensional reference structure is already known, but in many cases, this is impossible. 2) So from 2005 up to 2015, researchers begin to introduce machine learning algorithms to this area[8, 15, 16, 7, 17, 18, 19, 20, 21]. The application of machine learning classifiers allows users to get rid of generating template projections from reference volume, and users just need to pick a few real particles to train the classifiers[16, 7, 20]. Besides, some methods utilize pre-defined math functions to transform micrographs for detection, such as Difference of Gaussian (DoG) map[19] and image filtering to find edges[17]. The mainstream during this period is the combination of machine learning and template matching, resulting in [8, 15, 18, 21, 22], all of which have greatly reduced the workload in particle picking. However, either the machine learning classifier or template matching method still depends upon a certain level of human intervention during picking, a more intelligent method is still in urgent need. 3) In 2016 the first successful fully automated method is raised[6]. They are the first to apply the popular convolutional neural networks

(CNN) structure to capture the essential features of particles, and employ a cross-molecule training strategy to avoid any human interfering with the process of picking. But the computationally intensive nature of this approach brings intolerable picking time, about 1.5 minutes per micrograph. So there are still many things to improve.

In recent years, deep learning has revolutionized computer vision field, both in image classification[23, 24, 25] and object detection[23, 26, 27, 28]. Based on the promising success of deep CNN[25], Ross et al[28] proposed a simple and scalable algorithm in 2014 that significantly improved the object detection results, called Regions with CNN features (R-CNN). Next year, inspired by the Spatial Pyramid Pooling networks (SPPnets)[26], Ross put forward the Fast R-CNN which achieved a faster speed and higher mean average precision (mAP) on the Visual Object Classes(VOC) datasets[27]. Despite these breakthroughs in object detection field in the past few years, it still remains a blank about how to effectively port the Fast R-CNN technology to the particle picking problem and guarantee both accuracy and test speed in the fully automated cryo-EM micrograph analysis. So this is what our research attempts to answer.

In this paper, we apply the high accuracy and speed framework Fast R-CNN to these unclear and low contrast medical micrographs. Our program takes the original cryo-EM data as input (in MRC filetype), and convert it to BMP file, finally we can get the coordinates and scores of all bounding boxes containing good-quality protein particle. The coordinates are the positions of upper-left and lower-right corners of the bounding box, and the score is the probability of being proteins. With the help of cross-molecule training scheme raised by[6], we keep the fully automatic advantage. We have implemented our proposed method in Python based on Caffe[29] and Fast R-CNN[27] projects, and make it an open-source program, which can be downloaded from [30]. We have tested this program on the real cryo-EM micrographs of three molecules published in recent four years[3, 4, 5], and the results are very pleasant.

This paper is organized as follows. In Section 2, we present the related work about cross-molecule training scheme and Fast R-CNN framework. In Section 3, we describe our algorithm in detail, including data preprocessing, generation regions of interest, reduction of false positive, etc. In Section 4, we report our experiment results. Finally our discussion and conclusions are included in Section 5.

RELATED WORKS

2.1 Automatic Particle Picking based on Deep Learning

The detailed developments of particle picking methods can be found in INTRODUCTION. Among these methods the most relevant study to us is the DeepPicker[6]. In this deep learning approach, they trained a four-convolutional-layer CNN with the particle images and an equivalent number of negative samples, and the output was the score of a two-class softmax layer which generated the probability of being particles. During the test phrase, a fix-sized sliding window with a small step was applied to the micrograph, and then the images within the sliding windows would be put into the trained CNN. After an "Ice Cleaning" process, all images with a prediction score higher than 0.5 were marked as protein particles.

There is a key contribution in their research attracting us, that is the "Cross Molecule Training Strategy". They combined different already-solved particles from multiple types of other molecular complexes as the training dataset, which successfully captured the common abstract representation of latent features in protein particles. Thus the trained CNN net can be directly used to pick particles from the new micrographs without any human intervention. In this paper, we adopt this scheme for all trainings and testings.

2.2 Fast R-CNN

Fast R-CNN is short for "Fast Region-based Convolutional Network"[27], and it takes as input an entire micrograph and a set of regions of interest (RoI) instead of particle images within the sliding window. For each RoI of the micrograph, a delicate designed RoI pooling layer extracts a fixed-length feature vector from the feature map, which is computed from several convolutional and pooling layers. Then a sequence of fully connected layers is followed, transforms the feature vector and feeds it into two sibling output layers: one generates a softmax probability over all possible classes, and the other generates four real-valued numbers for each class as the RoI regression results. In this way, the Fast R-CNN framework applies the computationally intensive convolutional layer to the micrograph only once, achieving both accuracy and speed improvements.

We have noticed that a more elegant and effective solution called Faster R-CNN has been proposed. It significantly accelerates the RoI generation process for general object detection tasks, by introducing a "Region Proposal

Network” to Fast R-CNN substituting for the selective search method. We have tested this framework on the cryo-EM micrographs, but the result is unacceptable. We insist applying the Fast R-CNN not Faster R-CNN based on three reasons. Firstly, the region proposal network works terribly on the low contrast images, and the awful RoIs sharply reduce the recall and precision scores. Secondly, the size of possible particles is fixed in our task, normally 100×100 pixels, so the sliding window solution with an appropriate step length is our best choice. Finally, the generation of RoIs in sliding window method is extremely fast, e.g., less than 1 ms for 40k RoIs.

MATERIAL AND METHODS

3.1 Datasets and Data Preprocessing

Our dataset consists of micrographs from 3 protein molecules: human gammas-secretase[4], yeast spliceosome[3], and TRPV1[5], each of which has 100 micrographs in MRC filetype. The MRC micrograph is a common file format for structural biology, begins with some summary information such as the width and height, and then follows with a large sequence of pixel values in 4 bytes float. All the micrograph resolutions are about $4k \times 4k$, e.g. 3838×3710 . The human gammas-secretase and yeast spliceosome micrographs are obtained from Dr. Yigong Shi’s lab at Tsinghua University, and the TRPV1 dataset is downloaded from EMPIAR website with the entry ID EMPIAR-10005[31]. The detailed processes and settings when taking these pictures can be found in the original papers.

All the coordinates of reference protein particles, which were fed into Fast R-CNN as positive samples, were picked manually by one cryo-EM expert and then further verified by another two experts. To reduce the number of ice particles picked out by mistake, we trained the networks with 3 classes including protein particles, ice particles and background. The bounding boxes of ice particles were picked out by ourselves, which were easily recognized because of the dark brightness and weird shapes. The total number of ground-truth particles and ice particles is shown in Tab. 1, and our cross-molecule training scheme is shown in Tab. 2.

TABLE 1. The details in three datasets.

	Protein-Particles	Ice-Particles	Micrographs
Gammas	13,555	3,554	100
Spliceosome	9,678	9,902	100
Trpv1	16,115	1,577	100

TABLE 2. The cross-molecule training for 3 datasets.

Proteins in Training Set	Proteins in Testing Set
Spliceosome+Trpv1	Gammas
Gammas+Trpv1	Spliceosome
Gammas+Spliceosome	Trpv1

Since the pixel values of original micrographs are floating-point numbers with no limit on the range, the images are entirely dark and their dynamic ranges are very small. In Fig. 1 we can find that the poor quality of the original picture results from the long tail in the histogram, so we apply the histogram equalization to all micrographs included in our dataset. Specifically we define the histogram function(Eq. 1), density function(Eq. 2) and cumulative distribution function (CDF)(Eq. 2) as follows:

$$h(x) = \sum_{i=1}^n I(pixel_i \leq x), \quad x = 1, 2, \dots, \quad n \text{ is the total pixels} \quad (1)$$

$$p(x) = \frac{h(x)}{n}, \quad F(x) = \sum_{t=1}^x p(t) \quad (2)$$

According to the probability theory, we will get a uniform distribution after applying the CDF to itself:

$$newPixel_i = F(pixel_i) = \sum_{t=1}^{pixel_i} p(t) = \sum_{t=1}^{pixel_i} \sum_{j=1}^n \frac{I(pixel_j \leq t)}{n} \quad (3)$$

Then this histogram equalized data will be used to generate BMP images. Figure 1 shows that the revised picture has a broader dynamic range and higher contrast. We have compared the training loss before and after the adjustment in Fig. 3, and it shows that the histogram equalization wins a faster and better convergence result.

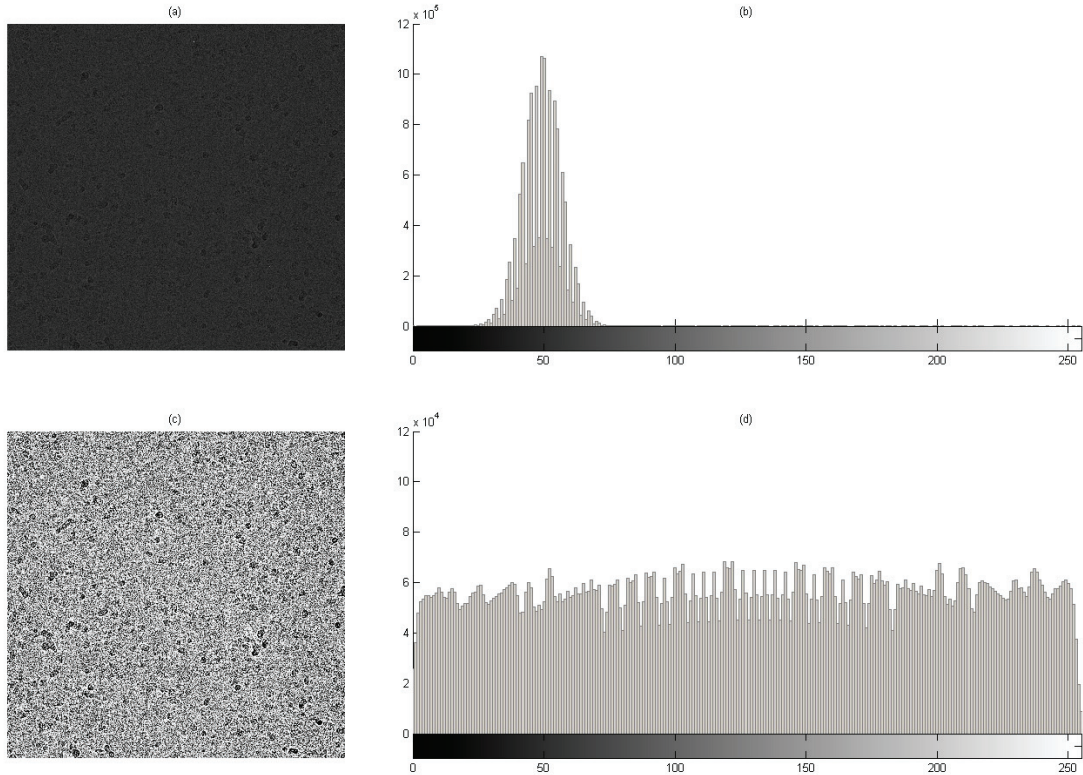


FIGURE 1. Data preprocess using Histogram Equalization. This example comes from Gammas protein.

3.2 Generation of Regions of Interest

With the improvement of the preparation method of protein solutions, the purity of cryo-EM samples is getting higher and higher. And our goal is to do a single-particle data analysis, so the targets in the micrographs have almost the same size, which can be easily estimated by the researcher and be set as our program parameter. For our dataset, all the three proteins use squares with a side length of 100 pixels, slightly larger than real particles. Since the target size in our object detection task is already set, the current advanced ROI (Region of Interest) generation technology can not be easily applied, which is also one of the reasons why we give up the Faster R-CNN framework. Considering about whether speed or effectiveness, the sliding window solution is our best choice.

We use a relatively small step size to slide over the entire micrograph, and the total number of RoIs is determined by Eq. 4. So how to choose a proper step size? We will use IoU (Intersection over Union) to measure the similarity between the final selected ROI and the ground-truth ROI in the evaluation process. In order to achieve higher IoUs, smaller steps should be used to obtain a more dense mesh. The relationship between the step size and the minimum IoU that it can guarantee is shown in Eq. 4, Eq. 5 and Eq. 8.

$$\text{number of ROI} = \lfloor (\text{width} - \text{BoxSide} + 1) / \text{step} \rfloor \times \lfloor (\text{height} - \text{BoxSide} + 1) / \text{step} \rfloor \quad (4)$$

$$\text{leastIntersection} = \min_{(\text{gtROI})} \left\{ \max_{(\text{ROI})} \text{Intersection}(\text{gtROI}, \text{ROI}) \right\} \quad (5)$$

$$= \min_{(0 \leq x, y \leq stepRate)} \left\{ [1 - \min(x, stepRate - x)] \times [1 - \min(y, stepRate - y)] \right\} \quad (6)$$

$$= (1 - \frac{1}{2} stepRate)^2 \quad (stepRate = step/BoxSide) \quad (7)$$

$$\text{least IoU} = \frac{\text{leastIntersection}}{2 \times 1^2 - \text{leastIntersection}} \quad (8)$$

Finally we chose 20% of the box side length as the step size, so it generated about 40,000 RoIs per micrograph and ensured a minimal IOU of 0.65. The test speed with different number of RoIs is measured, the result can be found in Fig. 6.

3.3 Reduction of False Positive

In the task of protein particle picking, the false positive outputs caused by ice are the common obstacle to a pleasant and useful solution. Figure 2(a) vividly illustrates the seriousness of the problem when we took no measures about the interference of ice particles, the green squares are particles recognized by our program as protein, and the red circles are the real particles picked manually. Instead of artificially setting up some rules to eliminate ice particles, we hand over this problem to our neural network to automatically learn the different features between ice and protein.

We use a three-class neural network instead of a binary classifier, and the outputs are probabilities over background, protein particles and ice particles, and regression coordinates for each category. As an initialization, we picked out manually all typical ice particles in the whole dataset, and formed a training set of 15,033 ice particles with the same box size as the protein. In the future learning, no manual work is needed, and researchers can use our training results to automatically pick ice particles from new micrographs and then add them to a new training set. Figure 2(b) shows the ice particles with blue squares picked by us, and (c) shows the results of a significant improvement.

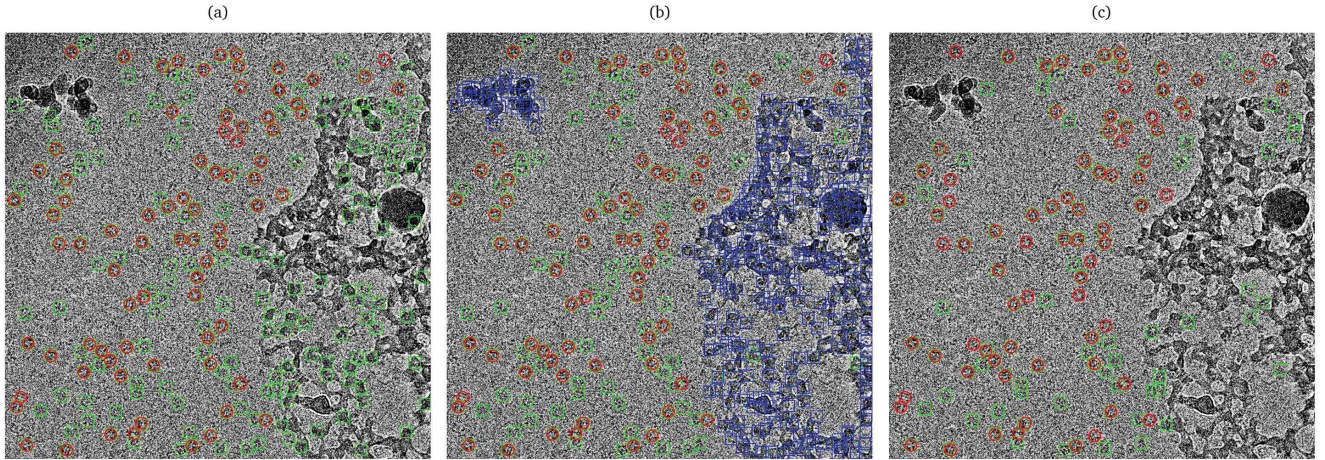


FIGURE 2. Results before and after ice reducing. This example comes from Trpv1 protein.

In addition to setting a separate category for ice particles, we also applied the Non-Maximum Suppression(NMS) to reduce false positives. In the process of ROI generation, the areas to be detected are seriously overlapping, which inevitably lead to lots of outputs in fact circle the same target. More importantly, if there is a false positive detection, a large number of duplicate false positives will appear around it. So in order to reduce redundancy, and to reduce the false positive, we apply the NMS technology after the top-k selection of RoIs sorted by the probability of being protein. In our NMS, all the other RoIs with a IoU higher than 0.5 will be deleted.

3.4 Details of Implementation

We applied the CNN called CaffeNet, essentially same as AlexNet[25]. The architecture of CaffeNet consisted of 5 convolutional layers, each of which was followed by a max pooling layer and an ReLU function. After the fifth

convolutional layer, the RoI-pooling layer[27] was applied, and then 2 fully connected layers with drop-out followed it. We adopted this neural network based on two reasons: firstly, the micrograph has no color information and the particle structure is simple and small, so there is no need to train a complex network; secondly, we are willing to use a pre-trained model and the trained CaffeNet based on ImageNet dataset is available on [32] and [33].

Then we fine-tuned this model on our dataset with a base learning rate of 0.0001, which decayed to one-tenth every 10,000 iterations. We trained 20,000 iterations in total on a Tesla K40c GPU, and it took us about 11 hours.

When tested a micrograph on our trained CaffeNet, we first selected the top 1000 RoIs according to the descending order of protein probability. Then we applied the NMS with a IoU threshold of 0.5 to them. A picked ROI is considered as True Positive if and only if it has a higher IoU than 0.65 with one ground-truth ROI, otherwise it is False Positive. The 0.65 is calculated by Eq. 8, with a fixed box size of 100 and a box generation step of $20\% \times 100$.

RESULTS

We evaluated all the essential processes of our particle picking solution, in a variety of indicators including training loss, test time, precision, recall, mAP and the average-IoU. We organized the main results in four parts as follows.

4.1 Evaluation in Training Loss

We introduced the Histogram Equalization as our data preprocessing, and the training losses before and after this transformation are shown in Fig. 3. All the loss values of equalized micrographs are lower than the original ones, meaning a better classification accuracy. Besides, the almost same wave shape means that the image after the transformation could maintain the original features. We trained the network for 20,000 iterations in total with two different learning losses, and it seemed to converge after just several thousands iterations within the first learning loss stage. So it is possible to achieve our accuracy in a shorter time.

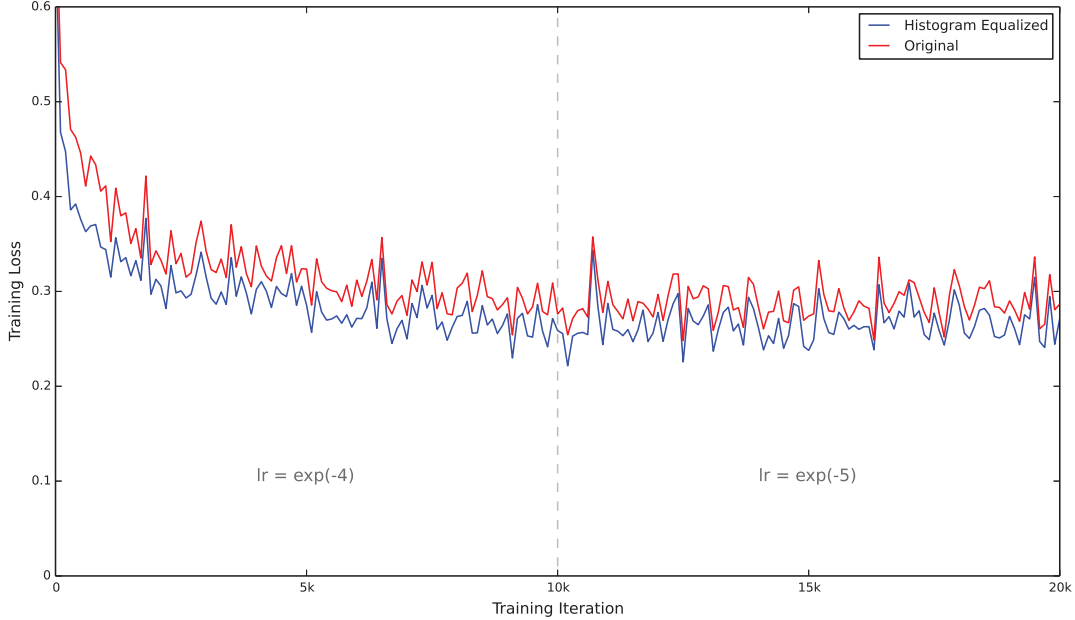


FIGURE 3. The Training Loss of Original Images and Histogram-Equalized Images. The training loss is a multinomial logistic loss, and the learning rate is 0.0001 for the first 10k iterations and then is 0.00001 for the next 10k. Each iteration took about 2 second, so we spent 11 hours in total for training one dataset.

4.2 Evaluation in Precision and Recall

After top-K selection and NMS process, the left RoIs are considered as our detection results. All these picked RoIs were separated into two parts: True Positives with a higher IoU than 0.65 with one ground-truth ROI, and False Positives without. The same separation was applied to all ground-truth RoIs, generating a new group called False Negative. Then the Precision and Recall were computed by Eq. 9 and Eq. 10.

$$Precision = \frac{TruePositive}{TruePositive + FalsePositive} \quad (9)$$

$$Recall = \frac{TruePositive}{TruePositive + FalseNegative} \quad (10)$$

In the task of protein particle picking, recall is always more important[6]. The purpose of the particle selection is to serve further studies, such as 3D reconstruction. Only by getting enough particles can we get a more accurate protein structure, so we expect to find out as many true particles as possible, to make full use of the micrographs captured. In Fig. 4, we choose the red dots on the three curves with high recall scores before the precisions decrease sharply. The detailed results can be found in Tab. 3, both the Precision and Recall are higher than the previous best result based on CNN in [6].

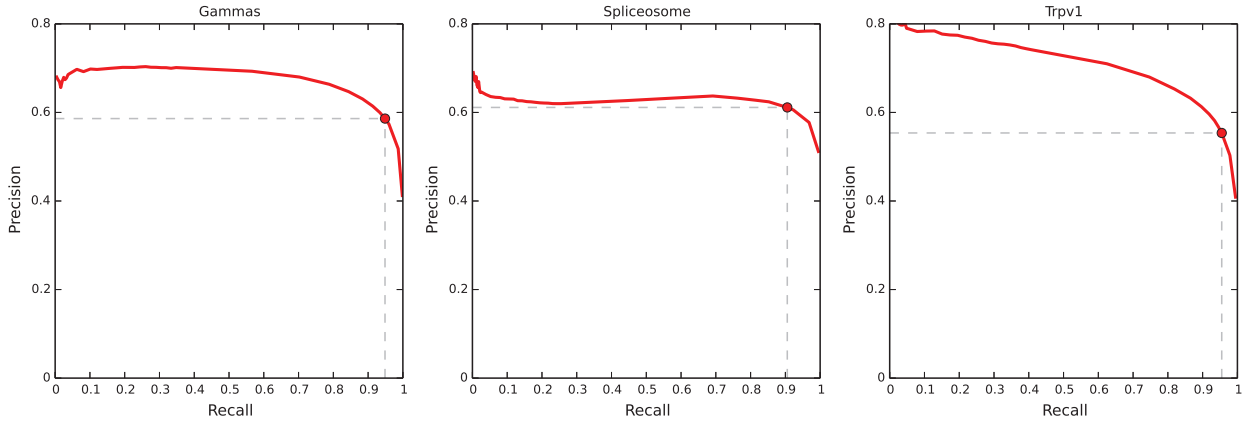


FIGURE 4. The Precision-Recall figures for three protein datasets. To obtain different pairs of recall and precision, we changed the top-K threshold from 1 to 1000. The red dots on these curves were our final choice (top-K = 1000).

TABLE 3. The detailed results for Gammas, Spliceosome and Trpv1 datasets.

	Recall	Precision	mAP	average-IoU
Gammas	0.9486	0.5861	0.7177	0.7486
Spliceosome	0.9055	0.6113	0.6944	0.7097
Trpv1	0.9549	0.5536	0.7486	0.7284

4.3 Evaluation in mAP and IoU

In addition to classical evaluation indices like Precision and Recall in the field of object detection, the mean-Average-Precision(mAP) and average-IoU are also used to evaluate. The average-IoU was calculated just for the True Positive detections by averaging all the IoUs between the TP ROI and Ground-Truth ROI. The results of mAP, Recall and average-IoU with different top-K settings are shown in Fig. 5.

For the first 10 settings of top-K in (a), the recall scores in the blue line increase linearly, which indicates the True Positive RoIs rank very high and the change of top-K contributes significantly to recall scores. In the meantime, the

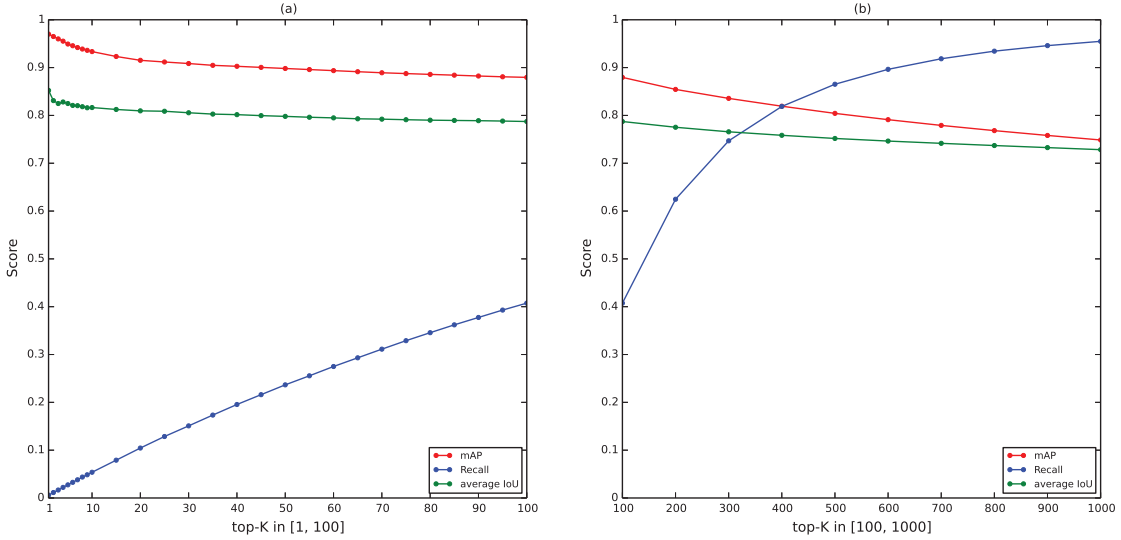


FIGURE 5. Evaluation in mAP and IoU with different top-K. The selection of K was not equidistant, so we represented the results in two separate figures with the same data definition. Each point in these figures correspond to an experiment.

mAP and average-IoU decrease slowly and keep higher than 0.8. For the larger settings in (b), the increase speed of recall is slower and slower, but it finally hits a very high recall. Even with the largest top-K, the mAP and average-IoU are still very high, making it possible for us to achieve a high recall without a big precision loss. The average-IoU is always higher than 0.7, which means a very precise prediction for the ground-truth RoIs and we can use the picked particles for further research with great confidence. In addition, the fluctuations of average-IoU with small top-Ks in (a) are worthy of our attention, and this phenomenon is the same as in Fig. 4, proving that too small top-Ks will lead to unstable results.

4.4 Evaluation of ROI Generation Method

As an important part of our method, the process of ROI generation significantly affects the final results. So We evaluated the impact of box-step settings from different angles in Fig. 6, including the total number of RoIs generated in (a), the average test time in (b), the least IoU guaranteed in (c) and the recall score in (d).

As shown in Fig. 6(a), the number of generated RoIs increases dramatically when box-step rate is less than 20%. And this makes it impossible for us to test on a single K40c GPU. From an economic point of view, we only consider the range of box-step rate higher than 20%. Besides, in (b), the larger box-step does not lead to significant speed improvements. Based on the current solution and network architecture, the test time for each micrograph is stable between 1 second and 2 seconds, which has greatly enhanced the speed of particle picking based on CNN[6]. The (c) is based on the Eq. 8, no matter how a ground-truth ROI falls in a tricky location, there is at least one generated ROI that has a higher IoU with it than the curve. For a box-step rate of 20%, 0.65 is guaranteed and 0.47 is guaranteed for 40%. The (d) shows the recall scores of experiments with different box-step, and when we use a denser box grid than 40%, we could obtain a score higher than 0.9. For the sake of better adaption to different protein data sets, we chose the 20% box-step rate with the highest recall. In short, to select an appropriate box-step, the memory limit of GPU and the desirable accuracy should come into consideration.

DISCUSSION

The main obstacle of automatic particle picking is the poor quality of cryo-EM micrographs. Different with the Electron Microscope used for metal, the cryo-EM is designed for biological materials which are easily damaged by electron beam. So the exposure time and dose are strictly limited, making the micrographs extremely blurred.

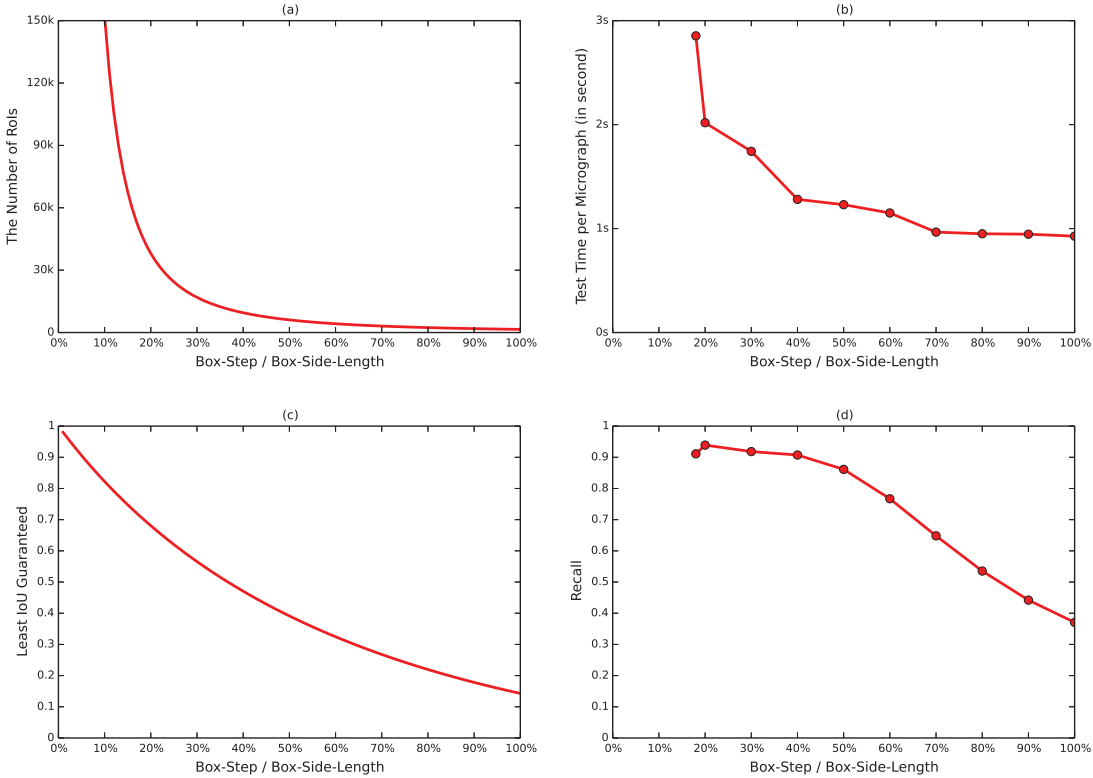


FIGURE 6. Evaluation of ROI Generation Method. The X axis ranging from 0 to 1, represents the ratio of box-step to box-side-length and we call it "box-step rate". For (a) and (c), the data was computed by Eq. 4 and Eq. 8, assuming the micrographs were in 4000×4000 and the box-side-length were 100. For (b) and (d), the data was from experiments. Due to the memory limit of Tesla K40c GPU(12 GiB), the smallest box-step rate we could apply was 18%.

Terribly, the less clear the picture is, the harder to pick particles automatically. We consulted researchers using cryo-EM, and they admitted that the particle selection is done by hand in practice, and it usually takes a few people to pick for a few days, even a week or two. So our work is in urgent demand.

Compared with general object detection tasks, our Precision score is not very high, just about 0.6. This may be partly resulted from the fact that researchers are more likely to mark locations with high confidence and ignore those with uncertainty, especially when doing such repetitive and tiring job. We can adjust the parameters to make Precision and Recall more balanced, however, the cryo-EM users prefer to accept a high Recall and endure the relatively low Precision.

In summary, the main contributions of our work are as follows. First, we are the first to successfully apply the Fast R-CNN framework to the Particle Picking task of cryo-EM micrographs, reducing the test time from 1.5 minutes to 2 seconds per image without any precision or recall loss. Second, we reduce the number of False Positive significantly by setting a single class for ice particles, and manually picked out all ice particles in the three datasets. Third, our picked ice particles and trained networks can be further applied to other protein datasets, in order to pick both protein and ice particles automatically and avoid any manual laborious work.

ACKNOWLEDGMENTS

We thank Prof. Yigong Shi and Xueming Li for generously sharing their cryo-EM micrographs. We are also grateful to Shizhen Xu and Zichuan Lin for their helpful discussions and encouragements.

REFERENCES

- [1] Y. Cheng, N. Grigorieff, P. A. Penczek, and T. Walz. A primer to single-particle cryo-electron microscopy. *Cell*, 161(3):438–449, 2015.
- [2] X. C. Bai, G. McMullan, and S. H. W. Scheres. How cryo-em is revolutionizing structural biology. *Trends in Biochemical Sciences*, 40(1):49–57, 2015.
- [3] C. Y. Yan, J. Hang, R. X. Wan, M. Huang, C. C. L. Wong, and Y. G. Shi. Structure of a yeast spliceosome at 3.6-angstrom resolution. *Science*, 349(6253):1182–1191, 2015.
- [4] L. F. Sun, L. Y. Zhao, G. H. Yang, C. Y. Yan, R. Zhou, X. Y. Zhou, T. Xie, Y. Y. Zhao, S. J. Wu, X. M. Li, and Y. G. Shi. Structural basis of human gamma-secretase assembly. *Proceedings of the National Academy of Sciences of the United States of America*, 112(19):6003–6008, 2015.
- [5] M. F. Liao, E. H. Cao, D. Julius, and Y. F. Cheng. Structure of the trpv1 ion channel determined by electron cryo-microscopy. *Nature*, 504(7478):107–+, 2013.
- [6] F. Wang, H. C. Gong, G. C. Liu, M. J. Li, C. Y. Yan, T. Xia, X. M. Li, and J. Y. Zeng. Deppicker: A deep learning approach for fully automated particle picking in cryo-em. *Journal of Structural Biology*, 195(3):325–336, 2016.
- [7] R. Norousi, S. Wickles, C. Leidig, T. Becker, V. J. Schmid, R. Beckmann, and A. Tresch. Automatic post-picking using mappos improves particle image detection from cryo-em micrographs. *Journal of Structural Biology*, 182(2):59–66, 2013.
- [8] R. Langlois, J. Pallesen, J. T. Ash, D. N. Ho, J. L. Rubinstein, and J. Frank. Automated particle picking for low-contrast macromolecules in cryo-electron microscopy. *Journal of Structural Biology*, 186(1):1–7, 2014.
- [9] R. M. Glaeser. Historical background: why is it important to improve automated particle selection methods? *Journal of Structural Biology*, 145(1-2):15–18, 2004.
- [10] N. Volkmann. An approach to automated particle picking from electron micrographs based on reduced representation templates. *Journal of Structural Biology*, 145(1-2):152–156, 2004.
- [11] V. Kumar, J. Heikkonen, P. Engelhardt, and K. Kaski. Robust filtering and particle picking in micrograph images towards 3d reconstruction of purified proteins with cryo-electron microscopy. *Journal of Structural Biology*, 145(1-2):41–51, 2004.
- [12] R. J. Hall and A. Patwardhan. A two step approach for semi-automated particle selection from low contrast cryo-electron micrographs. *Journal of Structural Biology*, 145(1-2):19–28, 2004.
- [13] A. M. Roseman. Particle finding in electron micrographs using a fast local correlation algorithm. *Ultramicroscopy*, 94(3-4):225–236, 2003.
- [14] W. V. Nicholson and R. M. Glaeser. Review: Automatic particle detection in electron microscopy. *Journal of Structural Biology*, 133(2-3):90–101, 2001.
- [15] J. H. Zhao, M. A. Brubaker, and J. L. Rubinstein. Tmacs: A hybrid template matching and classification system for partially-automated particle selection. *Journal of Structural Biology*, 181(3):234–242, 2013.
- [16] J. Vargas, V. Abrishami, R. Marabini, J. M. de la Rosa-Trevin, A. Zaldivar, J. M. Carazo, and C. O. S. Sorzano. Particle quality assessment and sorting for automatic and semiautomatic particle-picking techniques. *Journal of Structural Biology*, 183(3):342–353, 2013.
- [17] R. Langlois, J. Pallesen, and J. Frank. Reference-free particle selection enhanced with semi-supervised machine learning for cryo-electron microscopy. *Journal of Structural Biology*, 175(3):353–361, 2011.
- [18] P. Arbelaez, B. G. Han, D. Typke, J. Lim, R. M. Glaeser, and J. Malik. Experimental evaluation of support vector machine-based and correlation-based approaches to automatic particle selection. *Journal of Structural Biology*, 175(3):319–328, 2011.
- [19] N. R. Voss, C. K. Yoshioka, M. Radermacher, C. S. Potter, and B. Carragher. Dog picker and tiltpicker: Software tools to facilitate particle selection in single particle electron microscopy. *Journal of Structural Biology*, 166(2):205–213, 2009.

- [20] C. O. S. Sorzano, E. Recarte, M. Alcorlo, J. R. Bilbao-Castro, C. San-Martin, R. Marabini, and J. M. Carazo. Automatic particle selection from electron micrographs using machine learning techniques. *Journal of Structural Biology*, 167(3):252–260, 2009.
- [21] T. R. Shaikh, R. Trujillo, J. S. LeBarron, W. T. Baxter, and J. Frank. Particle-verification for single-particle, reference-based reconstruction using multivariate data analysis and classification. *Journal of Structural Biology*, 164(1):41–48, 2008.
- [22] J. Z. Chen and N. Grigorieff. Signature: A single-particle selection system for molecular electron microscopy. *Journal of Structural Biology*, 157(1):168–173, 2007.
- [23] C. Szegedy, W. Liu, Y. Q. Jia, P. Sermanet, S. Reed, D. Anguelov, D. Erhan, V. Vanhoucke, and A. Rabinovich. Going deeper with convolutions. *2015 Ieee Conference on Computer Vision and Pattern Recognition (Cvpr)*, pages 1–9, 2015.
- [24] M. D. Zeiler and R. Fergus. Visualizing and understanding convolutional networks. *Computer Vision - Eccv 2014, Pt I*, 8689:818–833, 2014.
- [25] Hinton G E. Krizhevsky A SI. Imagenet classification with deep convolutional neural networks. *Advances in neural information processing systems*, pages 1097–1105, 2012.
- [26] K. M. He, X. Y. Zhang, S. Q. Ren, and J. Sun. Spatial pyramid pooling in deep convolutional networks for visual recognition. *Ieee Transactions on Pattern Analysis and Machine Intelligence*, 37(9):1904–1916, 2015.
- [27] R. Girshick. Fast r-cnn. *2015 Ieee International Conference on Computer Vision (Iccv)*, pages 1440–1448, 2015.
- [28] R. Girshick, J. Donahue, T. Darrell, and J. Malik. Rich feature hierarchies for accurate object detection and semantic segmentation. *2014 Ieee Conference on Computer Vision and Pattern Recognition (Cvpr)*, pages 580–587, 2014.
- [29] Yangqing Jia, Evan Shelhamer, Jeff Donahue, Sergey Karayev, Jonathan Long, Ross Girshick, Sergio Guadarrama, and Trevor Darrell. Caffe: Convolutional architecture for fast feature embedding. In *22nd ACM international conference on Multimedia*, pages 675–678. ACM, 2014.
- [30] Yifan Xiao, 2016. <https://github.com/xiao1fan/FastParticlePicker>.
- [31] M. F. Liao, E. H. Cao, D. Julius, and Y. F. Cheng, 2013. <https://www.ebi.ac.uk/pdbe/emdb/empiar/>.
- [32] Caffe Models, 2016. <https://github.com/BVLC/caffe/wiki/Model-Zoo>.
- [33] Fast R-CNN, 2016. http://www.cs.berkeley.edu/~rbg/fast-rcnn-data/fast_rcnn_models.tgz.